Surface Deformation Evolution in the Pearl River Delta between 2006 and 2011 derived from the ALOS1/PALSAR images

Genger Li
Guangdong Institute of Surveying and Mapping of Geology
Guangcai Feng (fredgps@qq.com)
Central South University
Zhiqiang Xiong
Central South University
Qi Liu
Central South University
Rongan Xie
Guangdong Institute of Surveying and Mapping of Geology
Xiaoling Zhu
Guangdong Institute of Surveying and Mapping of Geology
Shuran Luo
Central South University
Yanan Du
Guangzhou University

Full paper

Keywords: Pearl River Delta, natural evolution, surface subsidence, SBAS-InSAR

Posted Date: October 30th, 2020

DOI: https://doi.org/10.21203/rs.3.rs-32256/v2

Version of Record: A version of this preprint was published on November 26th, 2020. See the published version at https://doi.org/10.1186/s40623-020-01310-2.

Abstract

This study monitors the land subsidence of the whole Pearl River Delta (PRD) (area: ~40,000 km^2) in China using the ALOS1/PALSAR data (2006-2011) through the SBAS-InSAR method. We also analyze the relationship between the subsidence and the coastline change, river distribution, geological structure as well as the local terrain. The results show that (1) the land subsidence with the average velocity of 50 mm/year occurred in the low elevation area in the front part of the delta and the coastal area, and the area of the regions subsiding fast than 30 mm/year between 2006 and 2011 is larger than 122 km^2; (2) the subsidence order and area estimated in this study are both much larger than that measured in previous studies; (3) the areas along rivers suffered from surface subsidence, due to the thick soft soil layer and frequent human interference; (4) the geological evolution is the intrinsic factor of the surface subsidence in the PRD, but human interference (reclamation, ground water extraction and urban construction) extends the subsiding area and increases the subsiding rate.

1. Introduction

Deltas have abundant natural resources, superior natural environment and geographical locations, so they accommodate the most intensive human activities. However, most deltas suffer from geological disasters caused by land subsidence, which damage buildings, railways, highways, subways and underground facilities (water supply pipes, gas and electrical installations), hindering the sustainable development in economy and environment (Ericson et al. 2006; Törnqvist et al. 2008; Wang et al. 2017). About 24 of the 33 major deltas in the world have surface subsidence, including the Pearl River Delta (PRD) in China (Syvitski et al. 2009). As one of the most economically developed and urbanized areas in China, the Pearl River Delta (PRD) has the largest urban agglomeration in the world and the population of 55 million. It has suffered many surface deformation disasters, including land subsidence, landslides and collapses (Syvitski et al. 2009; Chen et al. 2012; Ma et al., 2019).

The interferometric synthetic aperture radar (InSAR) technique has been widely used for monitoring surface subsidence in delta areas, including the PRD, because of its wide spatial and long temporal coverage (Higgins et al. 2014). Using C-band ENVISAT/ASAR data, Chen et al. (2012) mapped the surface deformation in the range of -15 to 15 mm/year from 2006 to 2010. Based on the X-band and COSMO-SkyMed data of Guangzhou and Foshan, Alex et al. (2018) monitored the surface deformation in the range of -35 to 10 mm/year between 2011 and 2017. Ma et al. (2019) investigated the subsidence of the Guangdong–Hong Kong–Macao Greater Bay Area and found that the overall subsidence ranged from 0 to 112.3 mm/yr derived from the 2015–2017 Sentinel-1 images. The results of these studies show similar subsidence patterns, but significantly different maximum subsidence orders (15 to 112.3 mm/y). Using a new kind of SAR dataset with long wavelength may address this controversy. The L-band ALOS1/PALSAR data have much longer wavelength than the C-band ENVISAT ASAR and X-band COSMO-SkyMed data, so it can detect much more reliable deformation information in densely vegetated area, like PRD. Therefore, we use ALOS1/PALSAR data to assess the order of the subsidence in PRD during 2006- 2011.

The surface deformation evolution in delta areas is contributed by both natural factors and anthropogenic interference. For the PRD area, many related studies focused on the local surface deformation caused by human activities, including ground water extraction and engineering construction (Wang et al. 2012; Chen et al. 2012; Xu et al. 2016; Wang et al. 2017; Alex et al. 2018). These studies provided a lot of useful information for understanding the local subsidence pattern in the PRD, but they paid little on the natural evolution factors, such as river distribution, coastline change and the local terrain.

In this study, we use the small baseline subset InSAR (SBAS-InSAR) method to map the surface deformation over the entire PRD (area: ~40,000 km^2) using 162 ALOS1/PALSAR images from 3 paths and 8 frames acquired between 2006 and 2011. The deformation results are verified by cross-validation of nearby path velocity rate and field investigation data. Then we analyze the temporal-spatial distribution characteristics of the deformation in the PRD, based on which we investigate the relationship between the subsidence and natural evolution factors as well as human interferences.

2. The Geological Background And Evolution Of The Prd

2.1 Geological background

The PRD is located in the south-central part of Guangdong province, bordering the South China Sea (Figure 1). It is an alluvial plain formed by the alluvium from the Xijiang River, Beijiang River and Dongjiang River (Huang and Zhang 2004). It covers an area of about 42, 200 km^2 from 112.5° to 114.25°E and 21.83° to 23.6°N. This delta is high in the north and low in the south, with small undulations. Influenced by the subtropical monsoon climate, the PRD has abundant rainfall and is often struck by typhoons and rainstorms. More than 300 river sections, with a total length of about 1740 km and an area of over 9,750 km^2, form a dense and complex network (Huang and Zhang 2004).

Bedrock (β), hidden karst (C), Quaternary loose soil (Q4) and soft soil form the geological structure of this area (Figure 2). The bedrock is mainly composed of granite and partially of metamorphic sandstone, clastic rocks and basalt. The hidden karst, composed of limestone and shale, concentrates in the Guanghua Basin. The Quaternary loose soil and soft soil form alluvial layers, which are thick in the front part (such as Zhongshan city and Nansha district of Guangzhou city) and thin in the rear part of the delta. These alluvial layers were formed between the Pleistocene and the Holocene (Zong et al. 2009), with the thickness of most parts varying from 5 to 36 m, and the maximum as 55 m. These soft layers mostly distribute along the river and in the flat terrain of the delta (Li et al. 1991).

2.2 River and coastline evolution of the PRD

The rich rainfall and abundant river flow carry sediments from the upper reaches to the lower reaches. The PRD is flat, so 20%~50% of the total sediment transport deposits in the river channel (Hu et al. 2011). Since the Tang dynasty, the population of the PRD started soaring. The agricultural development brought by the population growth accelerated the change of land use and led to serious soil and water loss. The

increased sediment discharge contributed to the growth of the estuarine delta and outward extending of the coastline (McManus 2002; Maselli and Trincardi 2013). In the past 6000 years, the coastline of the PRD has been pushed outward by 100 km (see Figure 2) (Fyfe et al. 1999; Zong et al. 2009).

Human activities also play an important role in the morphology and geomorphology evolution of the PRD, especially in the last 100 years. The influence of human activities even exceeded that of natural factors (Ericson et al. 2006; Syvitski and Satio 2007). And some researchers, based on the remote sensing images and historical maritime map, found that the reclamation is the main factor of the PRD morphology and geomorphology changes over the past 100 year (Seto and Kaufmann 2006; Li and Damen 2010; Wang et al. 2013).

3. Methodology And Results

3.1 SBAS-InSAR data processing

Given a differential InSAR pair acquired at moments t_A and t_B, the unwrapped phase is

$$\delta\phi_{obs} = \phi(t_B) - \phi(t_A) \approx \frac{4\pi}{\lambda}\Delta d + \frac{4\pi}{\lambda}\frac{B_{\perp j}\Delta z}{r\sin\theta} + \Delta\phi_{atm} + \Delta_{n_j} \quad (1)$$

where $\delta\phi_{obs}$ is the phase of one pixel in differential interferogram, Δd is the line of sight (LOS) deformation of a pixel between two images, Δz is the topographic error, $\Delta\phi_{atm}$ is the atmospheric delay phase, Δ_{n_j} is the phase noise. Equation (1) can be written in a matrix form as follows:

$$\begin{bmatrix} \frac{4\pi}{\lambda}\Delta t_1 & \frac{4\pi}{\lambda}\frac{B_{\perp 1}}{r\sin\theta} \\ \frac{4\pi}{\lambda}\Delta t_2 & \frac{4\pi}{\lambda}\frac{B_{\perp 2}}{r\sin\theta} \\ \vdots & \vdots \end{bmatrix} \begin{bmatrix} v \\ \Delta z \end{bmatrix} = \begin{bmatrix} \delta\phi_1 \\ \delta\phi_2 \\ \vdots \end{bmatrix} \quad (2)$$

where is the deformation rate. Following the SBAS-InSAR procedures (Berardino et al. 2002), we solve equation (2) by the least squares method, and obtain the linear deformation rate and the topographic error of each pixel. Subtracting topographic error and linear deformation phase from each differential interferogram, we get the residual phase. The residual phase consists of nonlinear deformation, atmospheric delay and noise. Taking the residual phase as the observation value, we obtain the time series phase of each SAR image by the singular value decomposition (SVD) method. We use the temporal high pass and spatial low pass filtering to obtain the atmospheric phase of each SAR image. Then,

atmospheric errors are subtracted from each interferogram. Finally, the SVD method is used to calculate time series of each pixel. Figure 3 shows the flowchart of the SBAS-InSAR method.

In this study, the L-band ALOS1/PALSAR data from 3 tracks are used to obtain the subsidence occurred in the PRD between 2006 and 2011 (see Figure 1, and Appendix (1)). The data are processed with the GAMMA software (Werner et al., 2003). The multi-look operation of 6 × 16 pixels in the range and azimuth directions is adopted to reduce phase noise and calculation burden before phase unwrapping. The result's resolution after multi-looking is about 50 m × 50 m. The interferometric pairs with the temporal baseline < 700 days and perpendicular baseline < 1000 m are selected to reduce the decorrelation. The topographic phase is removed using the 1-arcsecond (~30 m) Shuttle Radar Topography Mission DEM (Jarvis et al. 2008). A modified Goldstein filter is used to reduce noise phases (Li et al. 2008) and a mask with a coherence less than 0.4 is adopted to weaken the effect of low coherence regions (sea and isolated islands, etc.). Finally, the phase unwrapping is performed by the minimum cost flow algorithm (Mario 1998). The polynomial fitting is used to remove the long wave-length orbital errors in the unwrapped phase.

3.2 Surface subsidence results

Using the method described in section 3.1, we obtain the deformation rate map of the PRD between 2006 and 2011 (Figure 4). Figure 4a presents the average deformation rate derived from the ALOS1/PALSAR image. The hinterland is stable and the subsidence is mainly distributed in the front part of the delta and the coastal area. The average subsidence rate ranges from 10 to 50 mm/y, with the maximum deformation rate of >70 mm/y. Some regions have sporadic subsidence with a rate between 10 to 30 mm/y, such as the northeast part of Guangzhou city and the southeastern part of Zhaoqing city (outlined by the red dotted line in Figure 4).

Two large subsidence cones (S-1 and S-2 in Figure 4b) are observed in the front part of the delta. The most serious land subsidence is observed in the junction area of Zhongshan city and Jiangmen city (such as Jianghai district of Jiangmen city and Henglan town of Zhongshan city), with an area of 160 km^2. In this region, the subsidence rate of the center ranges from 30 to 50 mm/y, even >70 mm/y in some parts, and the average cumulative deformation is about 35 cm from 2006 to 2011 (Figure 4d). Subsidence cone S-2 covers Jinwan district of Zhuhai city and Tanzhou town of Zhongshan city, with an area of 230 km^2. Besides the two large subsidence cones, there are some areas with smaller subsidence rates, such as Doumen district of Zhuhai city and Xinhui district of Jiangmen city.

No large subsidence cone is found in the coastal areas. The subsidence areas scatter on the two sides of the Lingding Bay (see Figure 4c), such as Nansha district of Guangzhou city and Nanlang town of Zhongshan city and Tangjia town of Zhuhai city. The subsidence rate is between 20 and 40 mm/y, and is over 50 mm/y in some regions. The subsidence rates in the coastal areas of Dongguan and Shenzhen are smaller. For example, the subsidence rates of Chang'an town in Dongguan and Bao'an district in Shenzhen are 10 and 25 mm/y, respectively.

3.3 Results verification

In the verification, we compared the observations of Area1 and Area2 during the same period, which are the overlapping areas of Path 461 and Path 460 (Figure 4a). Area1 is stable but Area2 has obvious subsidence, so they can verify the results of different subsidence levels. As Figure 4e and f show, the velocity difference in Area1 is between -8 and 5 mm/y, and the overall mean value is -1.3 mm/y with a variance of 2.2 mm/y. In Area2, the velocity difference is between -10 and 6 mm/y, the mean value is -0.4 mm/y, and the variance is 3.8 mm/y. Because of decorrelation, atmospheric delays and different incidence angles, the results of the overlapping areas of adjacent paths, like Area1 and Area2, are slightly different, so the uncertainty (2.2 mm/yr and 3.8 mm/yr) between different paths is reasonable. To further verify the results, we did field investigations in some cities of the PRD, including Jiangmen city, Zhuhai city and Guangzhou city (see Figure 5). The filed observation confirmed the model results. To verify our result, we reprocessed the data using the IPTA method (Werner et al. 2003). The details of data processing and result comparison are shown in Appendix (2). The result comparison also confirms that the order and patterns of surface deformation are reliable.

4. Discussion

4.2.2 Geological structure

As shown in Figure 7, the areas located in bedrock distribution areas (β) (see Figure 7b) are very stable, and surface subsidence occurred in soft soil area. Before the modern delta were formed (6,000 years ago), the bedrock areas were isolated islands, and most of them were composed of bare rocks. As the coastline moved outward, those islands gradually merged into the land. So, the geological structures of these regions are stable. As Figure 7a and b show, there is a strong positive correlation between the thickness of the soft soil and the deformation rate. Higgins et al. (2014) drew the similar conclusion in the study of the subsidence of Ganges-Brahmaputra Delta. Therefore, the soft soil thickness can be inverted by the correlation between surface deformation and drilling data.

Soft soil is mainly distributed along rivers and in the low-lying areas of the delta, where the erosion caused by sea level rise is serious. In Figure 8a, the green area is lower than the average sea level, and it accounts for more than 1/3 of the entire onshore delta. The subsidence in the area below the sea level is outlined by the yellow line in Figure 8b. The comparison between Figure 8a and b shows that the land subsidence in the front and middle parts of the PRD concentrates in the area below the mean sea level. The annual average tidal range of the Pearl River Estuary is 1.0-1.7 m, and the load generated by tides and storm surges can cause settlements of a few millimeters to centimeters (Ye and Preiffer., 1990). The low-lying areas, affected by tides, sea level rise, storms and floods, are also the areas accommodating severe subsidence disasters. According to the Intergovernmental Panel on Climate Change (IPCC), the sea level had risen 0.19 m (1.7 mm/y) between 1901 and 2010. And the rise is accelerating (Zhang and Church 2012). These low-lying areas would suffer from both seawater erosion and surface subsidence in the future.

4.3 Human activities

4.3.1 Reclamation

In the 1960s, the large-scale reclamation in the PRD rapidly changed the shape of the coastline. The reclamation rate between 1970 and 1995 reached 21 km^2/y and then slowed down. We collect the coastline data from 1850 to 2015 with a time span of 165 years, and depict the changes in Figure 9. The blue line is the PRD coastline in 1850, and the red lines are the coastlines of different periods. In the past 165 years, the coastline and landforms have undergone tremendous changes. A large area of land has been reclaimed from waters and tidal flats. As the shoreline gradually moved towards the sea, more than 20 islands gradually merged into the mainland. By 2015, almost all the tidal flats in 1850 had been reclaimed into land.

As shown in Figure 9, the reclaimed areas are also the area with the largest subsidence rate (subsidence rate: >50 mm/y), including the coastal areas of Zhuhai, Guangzhou, Dongguan and Shenzhen. Most of these areas were reclaimed in the last 30 years (Xu et al. 2016; Huang and Zhang 2004), so the soil layers in these areas are unstable. Furthermore, the landfill materials are sediments, which causes subsidence by self-consolidation.

We select two areas, Nansha district of Guangzhou city and Jinwan district of Zhuhai city (outlined by the yellow dotted line in Figure 9) to analyze the relationship between the subsidence and reclamation in detail. As shown in Figure 10, these two areas were reclaimed from the sea a few decades ago. In 1984 (see Figure 10a), Longxue and Hengmen were small islands, but they gradually expanded outwards and formed the basic shape of the current island in 2016 (see Figure 10b-e). The area of Longxue island cofferdam grew about 150 times in 35 years. The newly reclaimed regions have serious subsidence, and the maximum subsidence rate is 75 mm/y (see Figure 10f). Figure 10g-k show the variation of the reclaimed region in Jinwan district of Zhuhai city, where two small subsidence cones are obvious (see Figure 10l). Gaolan island, which was an island before 2004, connected to the land in 2010 (see Figure 10j). The connection area accommodates the subsidence cones, where the maximum subsidence is 87 mm/y (see Figure 10).

Many countries, such as the Netherlands (Hoeksema 2007), the United Kingdom (Wali 1975), Japan (Suzuki 2003) and Singapore (Douglas and Lawson 2003; Xu et al. 2016), have reclaimed land from the sea for the coastal industries and agricultural development, as well as for storm defense. Surface deformation monitoring in the Nile Delta and the Tiber Delta indicates that the reclaimed area is the most severely subsiding area (Stramondo et al. 2008; Marriner et al. 2012). So the long-term monitoring of the reclaimed area in the PRD is necessary to ensure the safety of the construction there.

4.3.2 Other human interventions

The PRD region is an economic center of south China, where factories, buildings, farmlands, and fisheries are densely distributed. The deposits consolidation and reclamation are the main factors for the land

subsidence in deltas, but they alone cannot cause subsidence as high as 70 mm/y in small regions. We took the subsidence cone S-1(see Figure 4b) as an example to investigate the reason of local rapid subsidence. Through field investigation, we found that fish ponds are widely distributed in the coastal area of Jianghai (Figure 11a), where large area land subsidence occurred. Aquaculture needs great amount of freshwater. Aggressive extraction of groundwater leads to the rapid drop of the groundwater level and causes subsidence, even settlement cones. Two profiles along S-1 (Figure 11b), ab and cd, are used to show the settlement characteristics (Figure 11c and d).

The subsidence caused by excessive groundwater extraction is common in delta areas. In the Mekong Delta, the average land subsidence rate has reached 16 mm/y as more than 250,000 hectares of land has been converted from rice fields to shrimp ponds since 2000 (Erban et al. 2014). Oil and groundwater extraction play a key role in the land subsidence in the modern Yellow River Delta, and the land subsidence caused by aquaculture is up to 250 mm/y (Higgins et al. 2013). Therefore, we conclude that natural factors coupled with human activities cause the subsidence in the PRD. The evolution of the PRD determines the location of the subsidence areas, and human activities have become the direct cause of the settlement. Therefore, we should pay more attention to the subsidence caused by human activities.

5. Conclusions

We map the surface deformation of the entire PRD using the ALOS1/PALSAR images from 2006 to 2011. The results show that the areas with serious subsidence concentrate in the front part of the delta and the coastal areas. The two large settlement funnels in the front part of the PRD have the average settlement rates of 30-50 mm/y, and the maximum settlement rate of larger than 70 mm/y. The surface deformation map generated from the InSAR observation shows that: (1) the subsidence area is distributed along rivers; (2) the natural evolution would be the intrinsic factor for the land subsidence of the PRD; (3) the land subsidence in the PRD is significantly related to human activities (such as land reclamation, pumping groundwater for aquaculture). Due to the natural and human factors, the settlement in the PRD region will continue. These findings have guiding contributions to disaster prevention and social construction in the PRD.

Abbreviations

PRD: Pearl River Delta

Declarations

Ethics approval and consent to participate

Not applicable

Consent for publication

Not applicable

List of abbreviations

PRD: Pearl River Delta

Availability of data and materials

The ALOS/PALSAR data was provided by JAXA under Project PER2A2N038.

Competing interests

The authors declare no competing interests.

Funding

This research was supported by the National Key Research and Development Program of China under Grants 2018YFB0505500 and 2018YFB0505502, and National Natural Science Foundation of China (41574005).

Authors' contributions

Genger Li, Guangcai Feng, Zhiqiang Xiong, Qi Liu and shuran Luo conceptualized the manuscript and provided revision throughout the study. Genger Li, Guangcai Feng and Qi Liu drafted the manuscript. Zhiqiang Xiong, Qi Liu, Guangcai Feng and Yanan Du processed InSAR data. Genger Li, Rongan Xie, Xiaoling Zhu contributed to field work observation, the interpretations and discussion of the results.

Acknowledgements

We acknowledge the contributors for the GMT. We thank JAXA for providing ALOS1/PALSAR data under Project PER2A2N038.

Authors' information

Genger Li: senior engineer of Guangdong Institute of Surveying and Mapping of Geology.

Guangcai Feng: associate professor of Central South University, his research interest is surface deformation monitoring by using InSAR technology.

Endnotes

Not applicable

References

Alex H-MN, Wang H, Dai Y, Carolina P, Chen W, Ge L, Du Z, Zhang K (2018) InSAR Reveals Land Deformation at Guangzhou and Foshan, China between 2011 and 2017 with COSMO-SkyMed Data. Remote Sens 10:813. doi:10.3390/rs10060813

Aly MH, Klein AG, Zebker HA, Giardino JR (2012) Land subsidence in the Nile Delta of Egypt observed by persistent scatterer interferometry. Remote Sens Lett 3:621–630. doi:10.1080/01431161.2011.652311

Becker RH, Sultan M (2009) Land subsidence in the Nile Delta: Inferences from radar interferometry. Holocene 19:949–954. doi:10.1177/0959683609336558

Berardino P, Fornaro G, Lanari R, Sansosti E (2002) A new algorithm for surface deformation monitoring based on small baseline differential SAR interferograms. IEEE Trans Geosci Remote Sens 40:2375–2383. doi:10.1109/TGRS.2002.803792

Chen F, Lin H, Zhang Y, Lu Z (2012) Ground subsidence geo-hazards induced by rapid urbanization: Implications from InSAR observation and geological analysis. Nat Hazards Earth Syst Sci 12:935–942. doi:10.5194/nhess-12-935-2012

Douglas I, Lawson N (2003) Airport construction: Materials use and geomorphic change. J Air Transp Manag 9:177–185. doi:10.1016/S0969-6997(02)00082-0

Du Y, Feng G, Liu L, Fu H, Xing P, Wen D (2020) Understanding Land Subsidence Along the Coastal Areas of Guangdong, China, by Analyzing Multi-Track MTInSAR Data. Remote Sens 12:299. doi:10.3390/rs12020299

Erban LE, Gorelick SM, Zebker HA (2014) Groundwater extraction, land subsidence, and sea-level rise in the Mekong Delta, Vietnam. Environ Res Lett 9:084010. doi:10.1088/1748-9326/9/8/084010

Ericson JP, Vörösmarty CJ, Dingman SL, Ward LG, Meybeck M (2006) Effective sea-level rise and deltas: Causes of change and human dimension implications. Glob Planet Change 50:63–82. doi:10.1016/j.gloplacha.2005.07.004

Fyfe JA, Selby IC, Plater AJ, Wright MR (1999) Erosion and sedimentation associated with the last sea level rise offshore Hong Kong, South China Sea. Quat Int 55:93–100. doi:10.1016/S1040-6182(98)00030-5

Gebremichael E, Sultan M, Becker R, El Bastawesy M, Cherif O, Emil M (2018) Assessing Land Deformation and Sea Encroachment in the Nile Delta: A Radar Interferometric and Inundation Modeling Approach. J Geophys Res Solid Earth 123:3208–3224. doi:10.1002/2017JB015084

Higgins S, Overeem I, Tanaka A, Syvitski JPM (2013) Land subsidence at aquaculture facilities in the Yellow River delta, China. Geophys Res Lett 40:3898–3902. doi:10.1002/grl.50758

Higgins SA, Overeem I, Steckler MS, Syvitski JPM, Seeber L, Akhter SH (2014) InSAR measurements of compaction and subsidence in the Ganges-Brahmaputra Delta, Bangladesh. J Geophys Res F Earth Surf 119:1768–1781. doi:10.1002/2014JF003117

Hoeksema RJ (2007) Three stages in the history of land reclamation in the Netherlands. Irrig Drain 56. doi:10.1002/ird.340

Hu J, Li S, Geng B(2011) Modeling the mass flux budgets of water and suspended sediments for the river network and estuary in the Pearl River Delta, China. J Mar Syst 88:252–266. doi:10.1016/j.jmarsys.2011.05.002

Hu X, Lu Z, Wang T (2018) Characterization of hydrogeological properties in Salt Lake Valley, Utah, using InSAR. J Geophys Res Earth Surf 123:1257–1271. doi:10.1029/2017JF004497

Huang Z, Zhang W (2004) Impacts of artificial factors on the evolution of geomorphology during recent thirty years in the Zhujiang Delta. Quaternary Sciences 24:394-401.

Li P, Qiao P, Zheng H, Fang G, Huang G (1991) Environmental evolution in the Pearl River Delta over the past 10,000 years. China Ocean Press, Beijing (in Chinese).

Li X, Damen MCJ (2010) Coastline change detection with satellite remote sensing for environmental management of the Pearl River Estuary, China. J Mar Syst 82. doi:10.1016/j.jmarsys.2010.02.005

Li ZW, Ding XL, Huang C, Zhu JJ, Chen YL (2008) Improved filtering parameter determination for the Goldstein radar interferogram filter. ISPRS J Photogramm Remote Sens 63:621–634. doi:10.1016/j.isprsjprs.2008.03.001

Liu P, Li Q, Li Z, Hoey T, Liu Y, Wang C (2015) Land subsidence over oilfields in the Yellow River Delta. Remote Sens 7:1540–1564. doi:10.3390/rs70201540

Ma P, Wang W, Zhang B, Wang J, Shi G, Huang G, Chen F, Jiang L, Lin H (2019) Remotely sensing large- and small-scale ground subsidence: A case study of the Guangdong-Hong Kong-Macao Greater Bay Area of China. Remote Sens Environ 232. doi:10.1016/j.rse.2019.111282

Mario Costantini T (1998) A novel phase unwrapping method based on network programming. IEEE Trans Geosci Remote Sens 36:813–821. doi:10.1109/36.673674

Marriner N, Flaux C, Morhange C, Kaniewski D (2012) Nile Delta's sinking past: Quantifiable links with Holocene compaction and climate-driven changes in sediment supply? Geology 40:1083–1086. doi:10.1130/G33209.1

Maselli V, Trincardi F (2013) Man made deltas. Sci Rep 3:1926. doi:10.1038/srep01926

Mazzotti S, Lambert A, Van der Kooij M, Mainville A (2009) Impact of anthropogenic subsidence on relative sea-level rise in the Fraser River delta. Geology 37:771–774. doi:10.1130/G25640A.1

McManus J (2002) Deltaic responses to changes in river regimes. Mar Chem 79:155–170. doi:10.1016/S0304-4203(02)00061-0

Morton RA, Bernier JC, Barras JA (2006) Evidence of regional subsidence and associated interior wetland loss induced by hydrocarbon production, Gulf Coast region, USA. Environ Geol 50:261–274. doi:10.1007/s00254-006-0207-3

Jarvis, A., H.I. Reuter, A. Nelson, E. Guevara, 2008, Hole-filled SRTM for the globe Version 4, available from the CGIAR-CSI SRTM 90m Database (http://srtm.csi.cgiar.org).

Seto KC, Kaufmann RK (2006) Modeling the Drivers of Urban Land Use Change in the Pearl River Delta, China: Integrating Remote Sensing with Socioeconomic Data. Land Econ 79:106–121. doi:10.2307/3147108

Stramondo S, Bozzano F, Marra F, Wegmuller U, Cinti FR, Moro M, Saroli M (2008) Subsidence induced by urbanisation in the city of Rome detected by advanced InSAR technique and geotechnical investigations. Remote Sens Environ 112:3160–3172. doi:10.1016/j.rse.2008.03.008

Suzuki T (2003) Economic and geographic backgrounds of land reclamation in Japanese ports. Mar Pollut Bull 47:226–229. doi:10.1016/S0025-326X(02)00405-8

Syvitski JPM, Kettner AJ, Overeem I, Hutton EWH, Hannon MT, Brakenridge GR Day J, Vörösmarty C, Saito Y, Giosan L, Nicholls RJ (2009) Sinking deltas due to human activities. Nat Geosci 2:681–686. doi:10.1038/ngeo629

Syvitski JPM, Saito Y(2007) Morphodynamics of deltas under the influence of humans. Glob Planet Change 57:261–282. doi:10.1016/j.gloplacha.2006.12.001

Teatini P, Tosi L, Strozzi T(2011) Quantitative evidence that compaction of Holocene sediments drives the present land subsidence of the Po Delta, Italy. J Geophys Res Solid Earth 116. doi:10.1029/2010JB008122

Törnqvist TE, Wallace DJ, Storms JEA, Wallinga J, Van Dam RL, Blaauw M, Derksen MS, Klerks CJW, Meijneken C, Snijders EMA (2008) Mississippi Delta subsidence primarily caused by compaction of Holocene strata. Nat Geosci 1:173–176. doi:10.1038/ngeo129

Wali M (1975) Practices and Problems of Land Reclamation in Western North America. The University of North Dakota Press, Grand Forks.

Wang H, Feng G, Xu B, Yu Y, Li Z, Du Y, Zhu J (2017) Deriving spatio-temporal development of ground subsidence due to subway construction and operation in Delta regions with PS-InSAR data: A case study

in Guangzhou, China. Remote Sens 9:1004. doi:10.3390/rs9101004

Wang H, Wright TJ, Yu Y, Lin H, Jiang L, Li C, Qiu G (2012) InSAR reveals coastal subsidence in the Pearl River Delta, China. Geophys J Int 191:1119–1128. doi:10.1111/j.1365-246X.2012.05687.x

Wang XZ, Zhang HG, Fu B, Shi A (2013) Analysis on the coastline change and erosion-accretion evolution of the Pearl River Estuary, China, based on remote-sensing images and nautical charts. J Appl Remote Sens 7:073519. doi:10.1117/1.jrs.7.073519

Werner C, Wegmuller U, Strozzi T, Wiesman A (2003) Interferometric point target analysis for deformation mapping. IGARSS 2003. https://doi.org/10.1109/IGARSS.2003.1295516.

Wu ZY, Saito Y, Zhao DN, Zhou JQ, Cao ZY, Li SJ, Shang JH, Liang YY (2016) Impact of human activities on subaqueous topographic change in Lingding Bay of the Pearl River estuary, China, during 1955-2013. Sci Rep 6:37742. doi:10.1038/srep37742

Xu B, Feng G, Li Z, Wang Q, Wang C, Xie R (2016) Coastal subsidence monitoring associated with land reclamation using the point target based SBAS-InSAR method: A case study of Shenzhen, China. Remote Sens 8:652. doi:10.3390/rs8080652

Ye L, Preiffer KD (1990). Studies of 2D & 3D numerical simulation of Kelvin tide wave in Nei Lingdingyang at Pearl River Estuary. Ocean Engineering 8 (4), 33–44.

Zhang X, Church JA (2012) Sea level trends, interannual and decadal variability in the Pacific Ocean. Geophys Res Lett 39:L21701. doi:10.1029/2012GL053240

Zong Y, Yim WWS, Yu F, Huang G (2009) Late Quaternary environmental changes in the Pearl River mouth region, China. Quat Int 206:35–45. doi:10.1016/j.quaint.2008.10.012

Figures

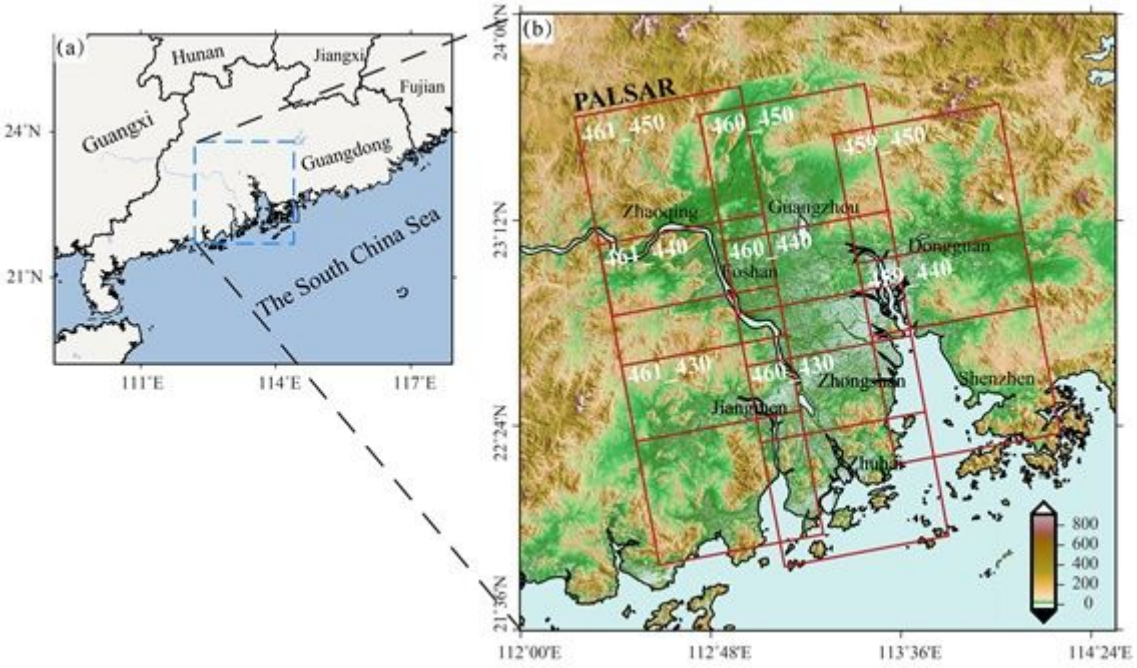

Figure 1

(a) Location and (b) the InSAR coverage of the study area. Red rectangles denote the InSAR image coverage and white numbers are the path and frame codes.

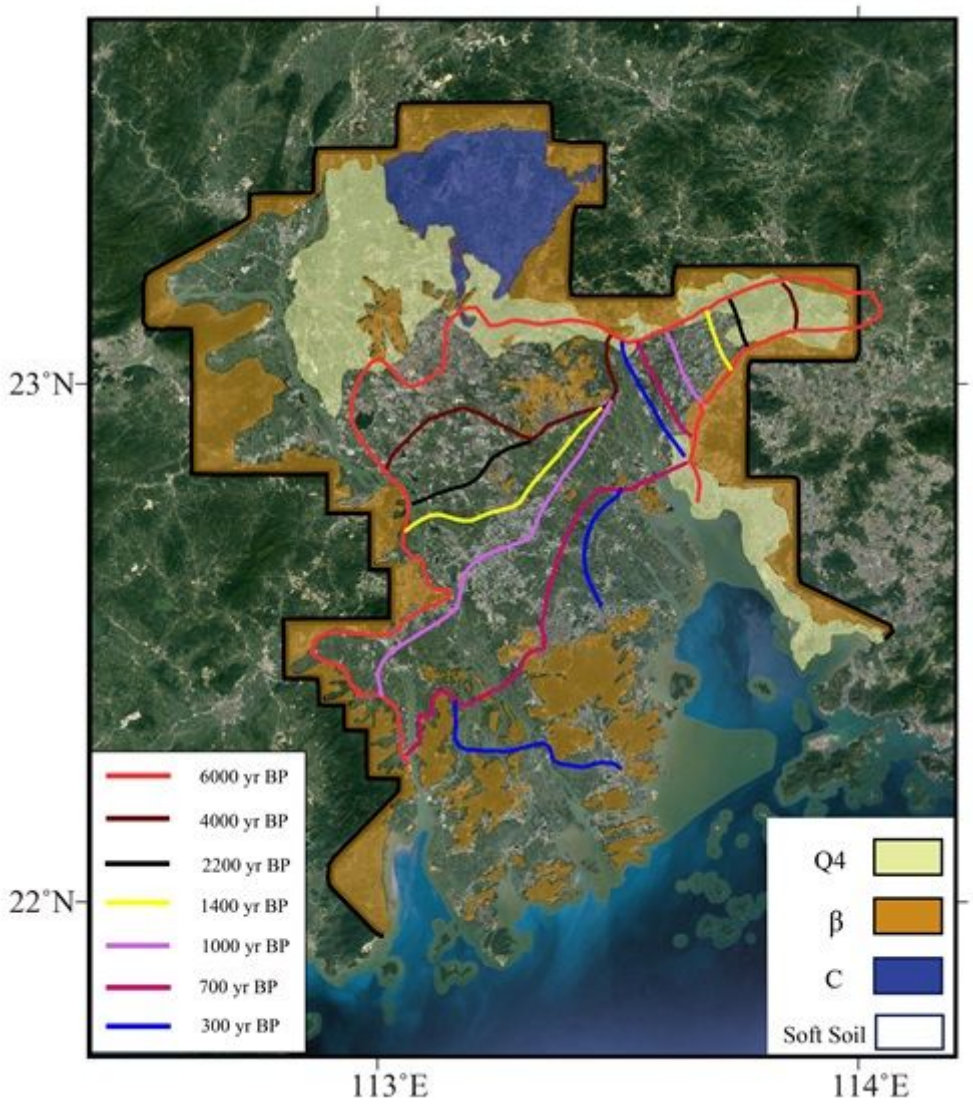

Figure 2

Geological formation map of the Pearl River Delta (PRD) (modified from Li et al. 1991). The colors inside the region outlined by the black line denote the Quaternary loose soil (Q4), bedrock (β), hidden karst (C), and soft soil. Curves of different colors represent coastlines of different time periods.

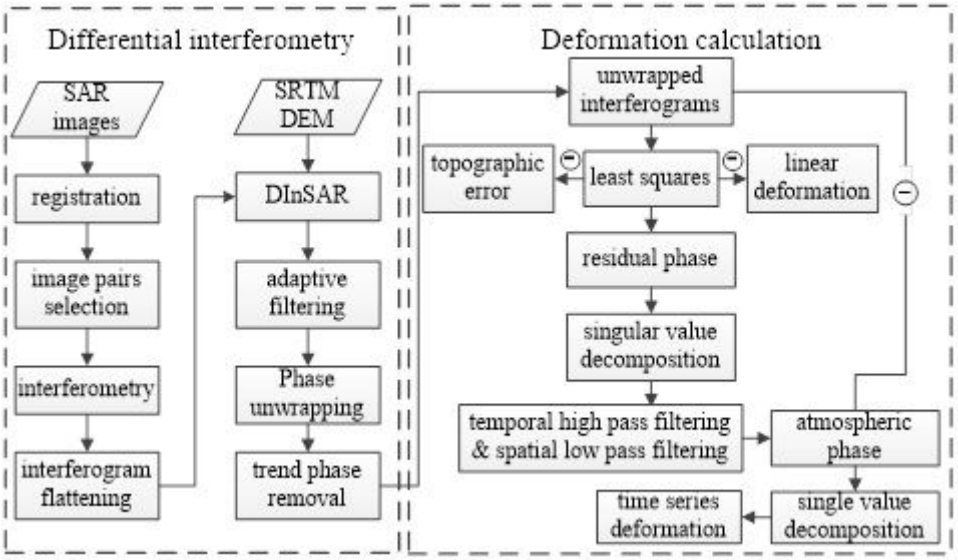

Figure 3

Flowchart of the SBAS-InSAR method used in this study.

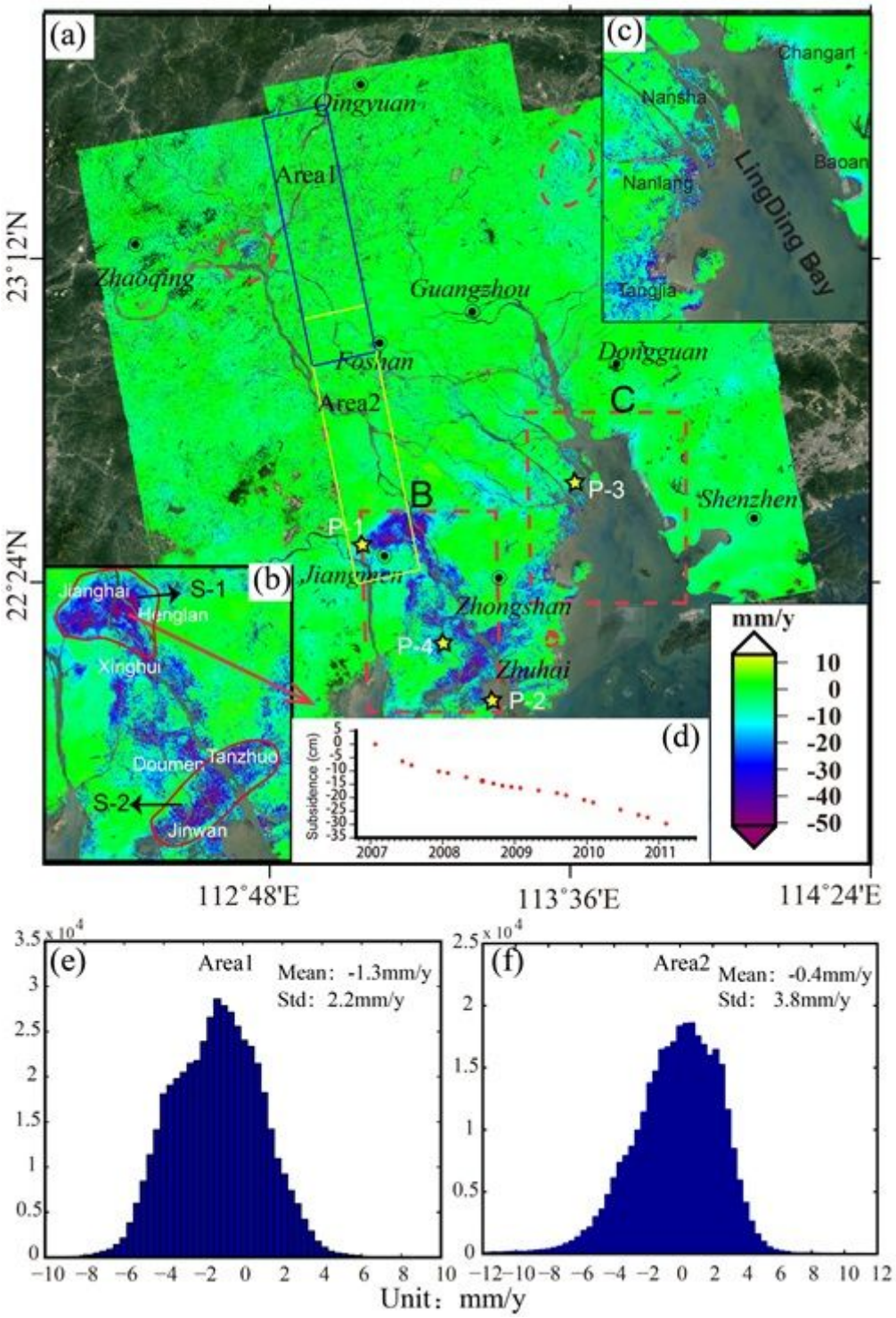

Figure 4

Surface deformation in the PRD estimated by SBAS-InSAR. (a) The deformation rate map from 2007 to 2011. The red dotted line outlines the subsidence area. The blue and yellow rectangles are the overlapping areas of paths 460 and 461 in frame 440 (Area1) and 450 (Area2), respectively. The field observation was carried out in the place marked by yellow stars. (b) and (c) are zoom-ins of areas B and C, respectively. S-1 and S-2 in (b) are two large subsidence cones. (d) the time series of the subsidence

cone S-1. (e) and (f) are the histograms of the difference of the average deformation rate of Area-1 and Area-2 derived from different frames, respectively.

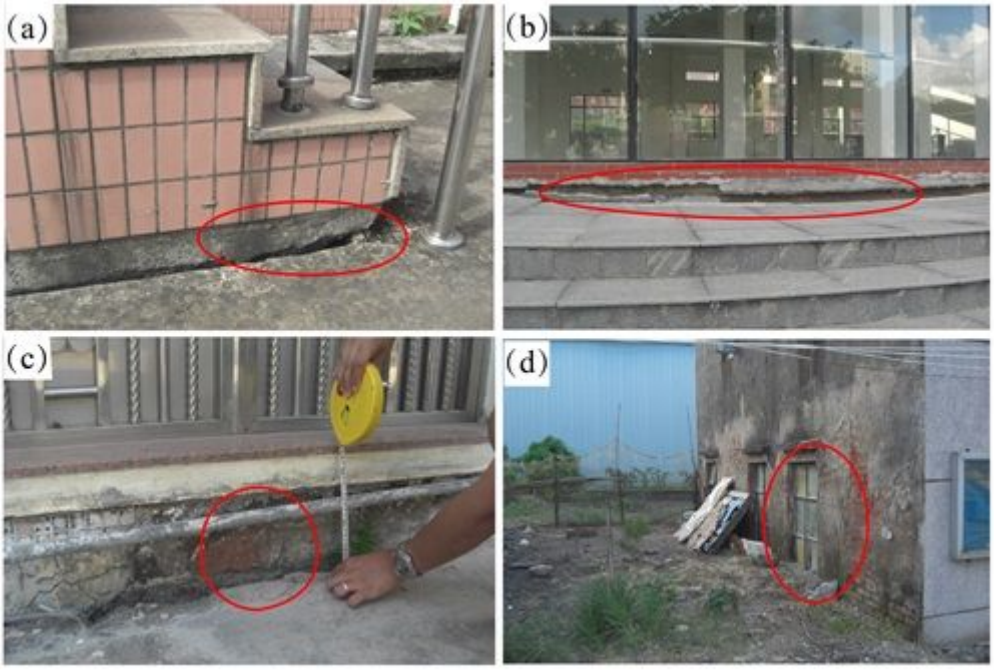

Figure 5

Photos of the filed investigation in the areas denoted by the yellow stars in Figure 4. (a) Xinhui port in Xinhui district, Jiangmen city (P-1 in Figure 4a). The ground subsided about 5 cm relative to the steps; (b) the Kangdelai Medical city in Jinwan district, Zhuhai city (P-2 in Figure 4a). The steps have separated from the building; (c) a building in Honghai village, Wanhaisha town, Nansha district, Guangzhou (P-3 in Figure 4a). The underground pipeline has exposed because of the ground subsidence; (d) a house in Sanban village, Hongqi town, Jinwan district, Zhuhai city (P-4 in Figure 4a). The windows have submerged into the ground.

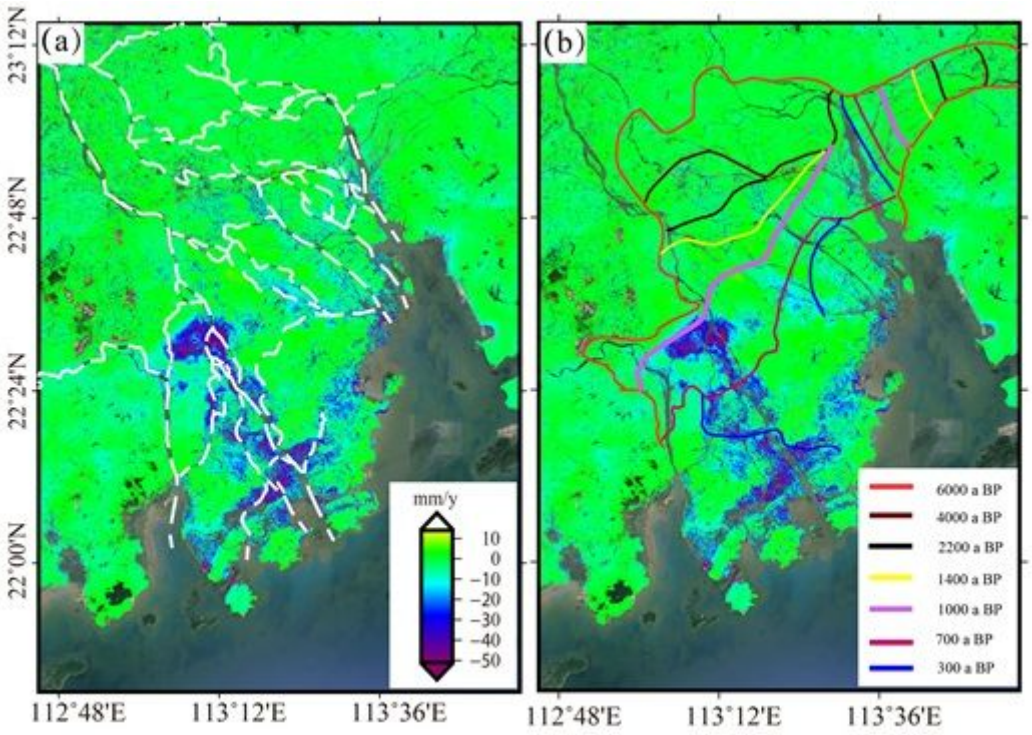

Figure 6

(a) Distribution map of the rivers in the PRD. The white dotted lines represent the rivers. (b) Coastlines of the PRD in the latest 6,000 years (modified from Li et al. 1991). The background is the average displacements velocity map of the PRD.

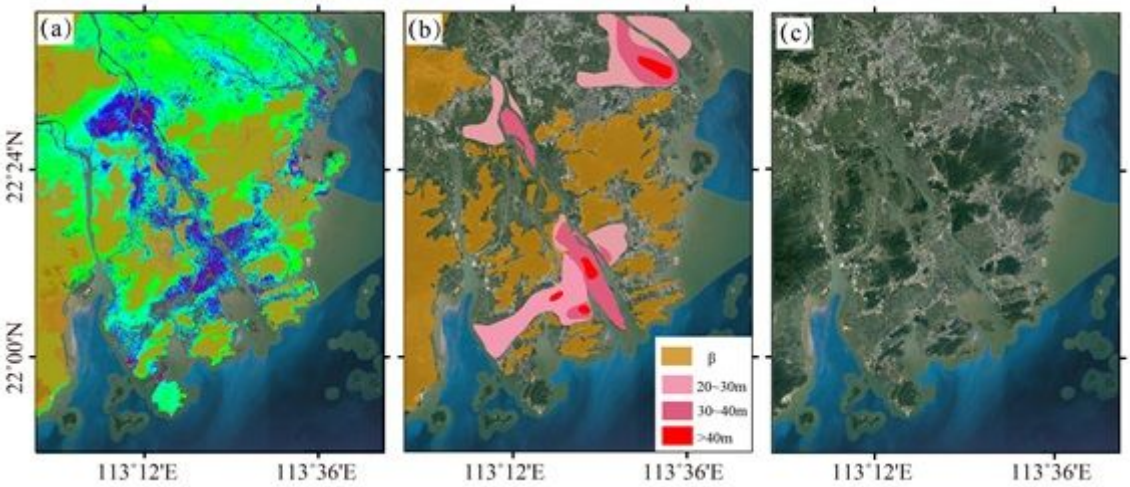

Figure 7

(a) The distribution of subsidence and bedrocks in the PRD, (b) soft soil thickness distribution in the PRD. β indicates the bedrock distribution; (c) optical imagery of interest area.

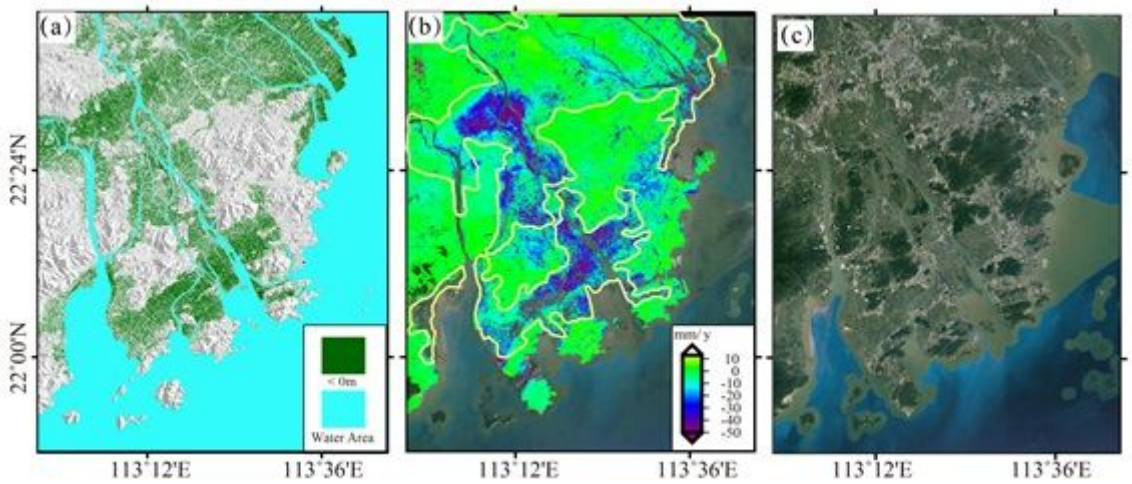

Figure 8

(a) DEM of the PRD. Green indicates the area below the average sea level; (b) Subsidence rate map of the PRD. The area below the mean sea level is outlined by the yellow line. (c) Optical imagery of interest area.

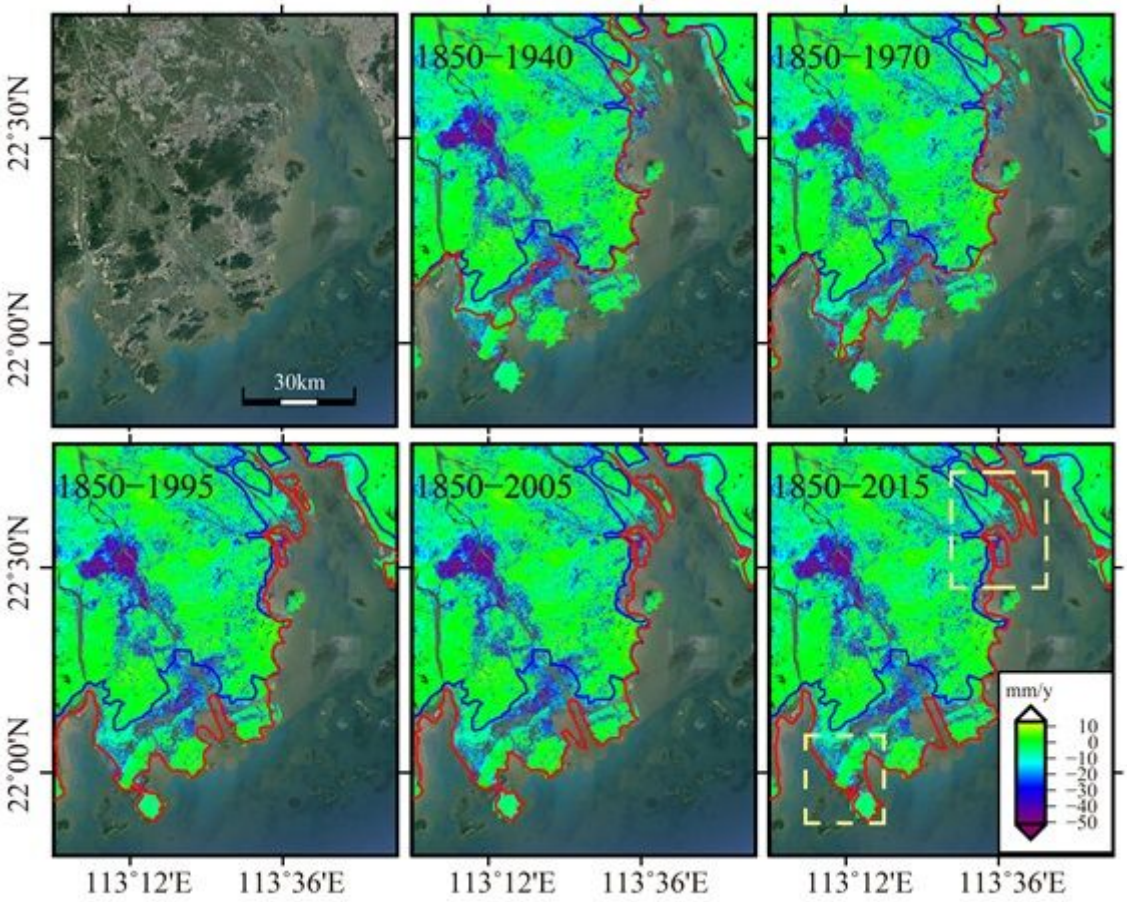

Figure 9

Optical image and the coastline changes in the PRD. The blue lines represent the coast line of the PRD in 1850, the red lines represent the coast line of the PRD in different time.

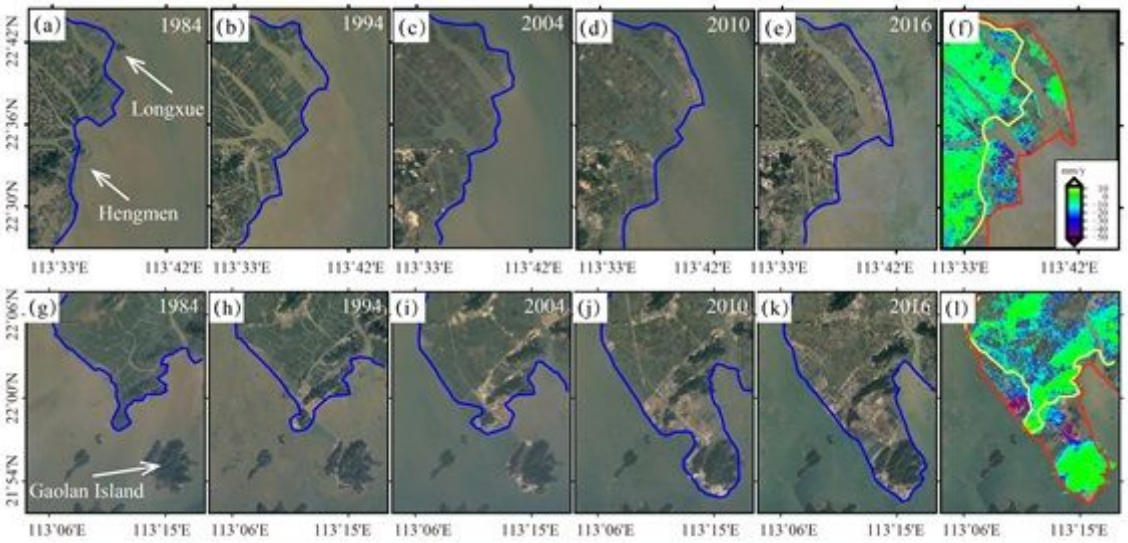

Figure 10

The cofferdam area change map and subsidence rate map of (a-f) Nansha District and (g-l) Jinwan District. The blue lines represent the coast line in different years. The yellow and red lines represent the coast line in 1984 and 2016, respectively.

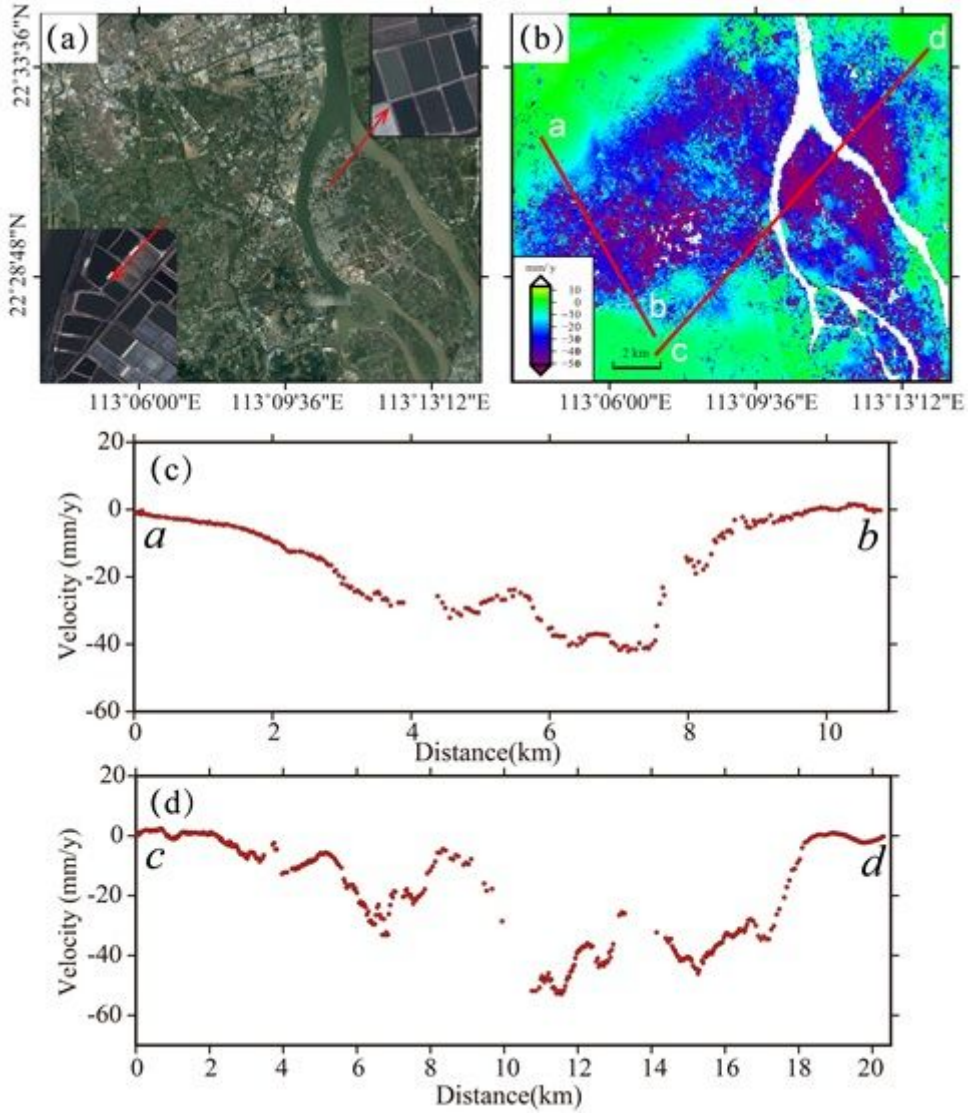

Figure 11

(a) Optical image of S-1 (Figure 4). The insets are the zoom-ins of the base map, where the fish ponds are clearly visible. (b) Average displacements velocity map of S-1. (c) and (d) are the average subsidence velocities of profiles ab and cd, respectively.

Supplementary Files

This is a list of supplementary files associated with this preprint. Click to download.

- GraphicalAbstract.png
- Appendix.pdf